Intrinsic Toroidal Rotation, Density Peaking, and Turbulence Regimes in the Core of Tokamak Plasmas

C. Angioni, R. M. McDermott, F. J. Casson, E. Fable, A. Bottino, R. Dux, R. Fischer, Y. Podoba, T. Pütterich, F. Ryter, E. Viezzer, and ASDEX Upgrade Team

Max-Planck-Institut für Plasmaphysik, IPP-EURATOM Association, D-85748 Garching bei München, Germany

(Received 7 September 2011; published 18 November 2011)

Observations in the ASDEX Upgrade tokamak show a correlation between the gradient of the intrinsic toroidal rotation profile and the logarithmic gradient of the electron density profile. The intrinsic toroidal rotation in the center of the plasma reverses from co- to countercurrent when the logarithmic density gradients are large, and the turbulence is either dominated by trapped electron modes or is at the transition between ion temperature gradient and trapped electron modes. A study based on local gyrokinetic calculations suggests that the dominant trend in the observations can be explained by the combination of residual stresses produced by $E \times B$ and profile shearing mechanisms.

DOI: 10.1103/PhysRevLett.107.215003 PACS numbers: 52.25.Fi, 52.35.Ra, 52.55.Fa

The transport of toroidal momentum in tokamak plasmas is presently receiving considerable attention [1,2]. Since the first observations [3,4], the intrinsic toroidal rotation, that is the toroidal rotation in the absence of any externally applied torque, has been considered an extremely interesting phenomenon of self-organization, by which the properties of plasma microturbulence produce a macroscopically measurable effect. As such, the phenomenology observed in tokamaks can also be of interest to other fields, like fluid dynamics or astrophysics, where processes of self-organization can occur [5]. Reversals of the intrinsic toroidal rotation in the plasma center from cocurrent to countercurrent as a consequence of a small change in plasma parameters (usually plasma density) present a particularly interesting class of observations [6–10].

Because of a recent upgrade of the charge exchange spectroscopy diagnostic system in ASDEX Upgrade (AUG), during the last experimental campaign more than 200 observations of intrinsic toroidal rotation profiles were made and have been organized into a database [11]. Large variation of densities (from 1 to 8.5×10^{19} m^{-3}), currents (from 0.4 to 1 MA), edge safety factors (from 2.9 to 10), and heating powers (from OH up to 3 MW electron and 5 MW ion cyclotron heating) are included. All of the plasmas are in lower single null configuration. This allows an unprecedented study of the dependences of the intrinsic toroidal rotation profile on theoretically relevant plasma parameters and a comparison with the dependences predicted by most recent theoretical models. In Fig. 1 the Mach number in the central region of the plasma, $M = R\Omega/v_{thi}$, is shown to have an extremely high correlation (94%) with the normalized toroidal rotation gradient, $u' = -(R^2/v_{thi})d\Omega/dr$, at midradius. Here, Ω is the toroidal angular velocity of the plasma and $v_{thi} = \sqrt{2T_i/m_i}$. This correlation holds for all of the plasma scenarios considered in this study, which include Ohmic heated, electron and ion cyclotron heated plasmas in the low confinement mode (L mode), and electron and ion cyclotron heated plasmas in the high confinement mode (H mode) of tokamak operation. In particular, no difference is observed between L modes and H modes, and in both confinement modes both positive (cocurrent) and negative (countercurrent) central rotation can occur. In both confinement modes, these reversals of the central intrinsic toroidal rotation are determined by the behavior of the toroidal rotation profile in the confinement region, around midradius. This behavior in the core is not influenced by the behavior of the toroidal rotation at the edge, which shows relatively limited variation over the entire set of observations. This result appears to disagree in part with some recent conclusions based on previous observations [10,12], which propose a separation between the behaviors in L mode and H mode [10]. However, in our understanding, the new observations

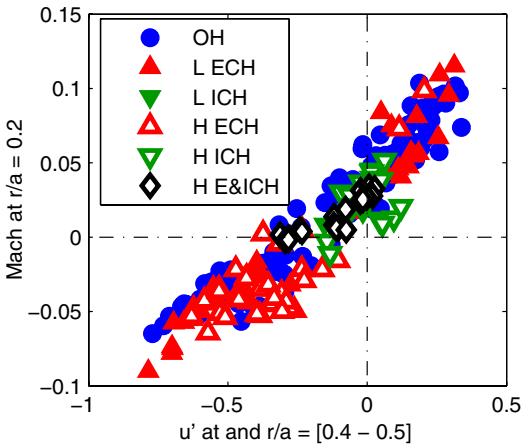

FIG. 1 (color online). Mach number at $r/a = 0.2$ versus the normalized gradient u' at $r/a = 0.45$ in L and H modes with OH and with auxiliary ion (ICH) and electron cyclotron heating (ECH).

from AUG reported here provide a complementary, and important, additional piece of information, since they cover a parameter domain with dominant electron heating. As many of the previous observations were made in plasmas with a significant fraction of ion heating, this suggests that a separation should be more generally made between dominantly ion heated and dominantly electron heated plasmas, rather than between L mode and H mode. In the database considered here, variation of the edge ion temperature, which has been recently identified as the main parameter affecting the edge plasma rotation [13,14], remains relatively limited. This also implies that the present database is particularly well suited for the analysis of the behavior of the intrinsic toroidal rotation in the plasma core.

Motivated by the correlation observed in Fig. 1, we study the dependences of u' on several dimensionless local plasma parameters around midradius, with the goal of identifying the main parameters with which it is correlated. To this end, in Fig. 2(a) the normalized toroidal rotation gradient u' at $r/a = 0.45$ is plotted as a function of the local normalized collisionality $\nu_{\rm eff} = \nu_{ei}/(c_s/R)$, where ν_{ei} is the electron ion collision frequency and c_s is the sound speed. We observe that u' exhibits a nonmonotonic dependence, also crossing zero, reminiscent of observations of rotation reversals observed in other devices [6–10]. In Fig. 2(b), the normalized logarithmic density gradient $R/L_{ne} = -R\nabla n_e/n_e$ exhibits an almost specular nonmonotonic dependence as a function of $\nu_{\rm eff}$. The density profile reaches a maximum peaking around $\nu_{\rm eff} \approx 0.5$, which corresponds to the same collisionality range where u' reaches the minimum values. In Fig. 2(c) R/L_{ne} is plotted as a function of the edge safety factor q_{95}, which shows that the large variation of density peaking observed in this collisionality range turns out to correlate with the increase of q_{95}. Because of the dominant auxiliary electron heating in all these cases, the electron to ion temperature ratio T_e/T_i shows a very strong dependence on $\nu_{\rm eff}$. Finally, Fig. 2(d) shows u' as a function of R/L_{ne}, which is the dimensionless local parameter with which u' exhibits the highest correlation (70%). The observed correlation with R/L_{ne} suggests an investigation of the turbulent regimes likely to be present in all of these plasmas, since studies on particle transport showed that the behavior of the electron density profile is strongly connected with the type of turbulence [15].

On the basis of these considerations, local linear gyrokinetic calculations have been performed with the code GS2 [16] for each observation in the database, in order to identify the dominant unstable mode at the typical binormal wave number $k_y\rho_i = 0.3$. The actual measured local data at $r/a = 0.45$ for every case were used as inputs for the code. The results of these calculations are applied to plot R/L_{ne} and u' as a function of the real frequency of the most unstable mode in Fig. 3. The type of instability is strongly determined by collisionality, T_e/T_i, and by the logarithmic temperature gradients, which implies that Fig. 3(a) appears similar to Fig. 2(b). Density peaking shows a nonmonotonic behavior as a function of the mode real frequency ω_r, reaching maximum values when ω_r is negative, when the mode propagates in the electron drift direction, at moderate absolute value. Negative values of the real frequency identify trapped electron modes (TEM), in contrast to positive values, which identify ion temperature gradient (ITG) modes. The present result is consistent with previous specific studies on particle transport [17–20], where the behaviors of thermodiffusive and convective particle fluxes have been studied as a function of the dominant instability and as a function of collisionality. In particular, the nonmonotonic dependence observed in Fig. 3 is matched by the theoretical predictions of Fig. 7 in [19], where the increase of peaking with increasing q_{95} shown in Fig. 2(d) was also predicted to be produced by an

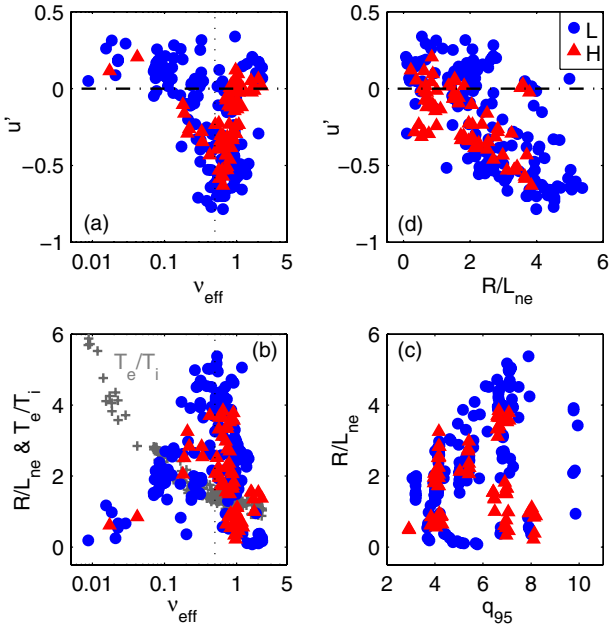

FIG. 2 (color online). u' (a), R/L_{ne} and T_e/T_i (b) versus $\nu_{\rm eff}$ (all at $r/a = 0.45$), R/L_{ne} at $r/a = 0.45$ versus q_{95} (c), and u' versus R/L_{ne} (d) (both at $r/a = 0.45$).

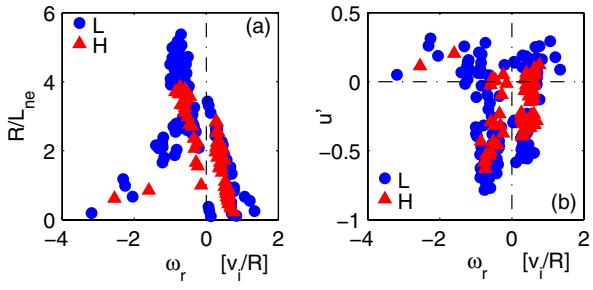

FIG. 3 (color online). R/L_{ne} (a) and u' (b) at $r/a = 0.45$ versus the real frequency ω_r of the most unstable mode at $k_y\rho_i = 0.3$.

increase of magnetic shear in the TEM domain. Fluctuation measurements which identify the turbulence regime present in these plasmas are not available. However, the consistency between present gyrokinetic results and previous knowledge on particle transport gives confidence in the fact that the linear gyrokinetic analysis correctly identifies the dominant turbulence type occurring at least in the majority of the plasmas considered here. In Fig. 3(b), no clear correlation between u' and the real frequency ω_r can be observed for the database as a whole. However, it appears that the cases which have the largest negative values of u' are either in the TEM domain or close to the transition between TEM and ITG. In addition, the observations which have the largest negative frequencies, deeply in the TEM instability domain, do not have large negative values of u'. These cases are characterized by very large values of T_e/T_i, large values of the logarithmic electron temperature gradient, and the smallest values of ν_{eff}. By combining the results shown in Figs. 2 and 3, it can be concluded that the intrinsic toroidal rotation develops positive gradients (that is hollow profiles) which can lead to countercurrent toroidal rotation in the center in conditions when the density profiles are sufficiently peaked. These conditions correspond to a turbulence regime which is either in the TEM domain, or close to the ITG-TEM transition. Otherwise, and particularly when the turbulence regime is deeper in the TEM domain, the toroidal rotation profile does not become hollow and the central rotation does not reverse to countercurrent, because in these conditions the density profiles are flatter.

A combined analysis on particle and electron heat transport on AUG [17] related the transitions from TEM to ITG to the behavior of the peaking of the electron density profiles and to the transition from linear Ohmic confinement (LOC) to saturated Ohmic confinement (SOC), consistent with past and more recent studies [21,22]. Recently, a correlation between LOC and SOC regimes and the occurrence of reversals of the intrinsic toroidal rotation has been found in Alcator C-Mod [10]. These considerations motivated a similar analysis of the AUG database. A subset of observations in our present database provides a density scan in OH L mode at 1 MA plasma current. The behavior of this subset is presented in Figs. 4(a) and 4(b), where the energy confinement time and the central value of the Mach number are plotted as a function of collisionality. As shown also by the profiles in Fig. 4(c), in the LOC regime the central Mach number is observed to have positive values (cocurrent) at very low density, deep in the TEM instability domain, while it becomes negative (countercurrent) close to the transition from LOC to SOC, and therefore close to the transition from TEM to ITG. In the SOC regime, the central Mach number reverses to cocurrent when the turbulence regime is deep in the ITG domain. The rather puzzling observation of a double sign reversal of the central rotation with increasing density can

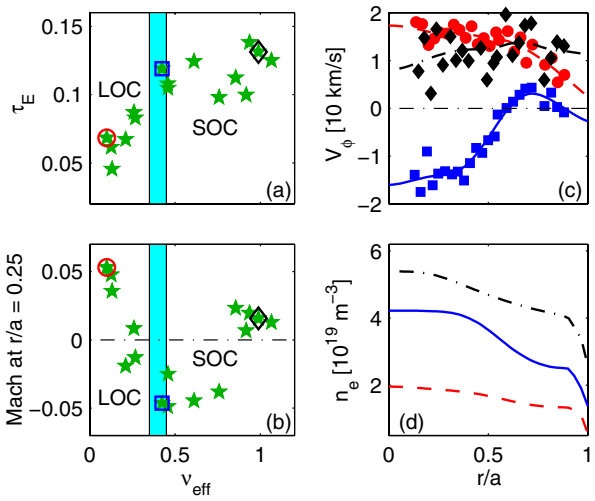

FIG. 4 (color online). Confinement time (a) and Mach number (b) at $r/a = 0.25$ as a function of ν_{eff} and toroidal rotation (c) and density (d) profiles of three cases identified by correspondent big open symbols in (a) and (b).

find an explanation if the criterion to obtain a countercurrent rotation is associated with the correspondence between the behavior of the density profiles and the turbulence regimes. Indeed, as shown in Fig. 4(d), during the early phases of the density ramp the density profile is less peaked, likely due to density pumpout which occurs in strong TEM turbulence. At intermediate densities, close to the LOC to SOC transition, and therefore close to the transition to ITG, the density profile becomes more peaked, and strong central countercurrent rotation is observed. At higher density (and higher collisionality), in the SOC regime dominated by ITG, the density peaking is reduced, as is the hollowness of the toroidal rotation profile. Hence, the analysis of a LOC to SOC transition confirms the connection between the behavior of the density profile and the intrinsic toroidal rotation, consistent with the conclusion drawn from the analysis of the entire database.

Several mechanisms have been proposed theoretically to identify sources of residual stress and explain the observation of intrinsic toroidal rotation in tokamaks [2]. The residual stress Γ_{RS} is the part of the radial flux of toroidal momentum Γ_ϕ which is not proportional to toroidal velocity nor to its gradient; that is,

$$\Gamma_\phi = \chi_\phi u' + RV_\phi u + \Gamma_{\text{RS}}.$$

Specifically, the mechanisms produced by the parallel perpendicular Reynolds stress in the core $\langle \tilde{v}_\parallel \tilde{v}_{E\times B,r} \rangle$, due to the shearing of the $E \times B$ flow [23–27] and of the profiles [27–29], can be expected to be relevant here. A critical requirement for theory to be at least qualitatively consistent with the experimental observations is that the residual stress becomes small when the logarithmic density gradient is small.

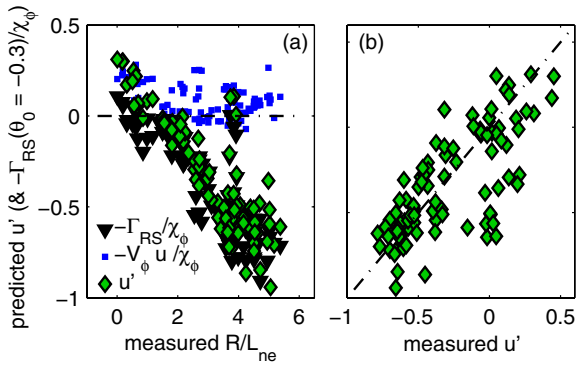

FIG. 5 (color online). Local GS2 linear calculations of the contributions to u', due to Γ_{RS}, assuming a tilting angle of -0.3 rad (triangles pointing down), and from the Coriolis pinch (small squares), versus measured R/L_{ne} (a), and the predicted values of u' (diamonds) versus measured R/L_{ne} (a) and u' (b), in the TEM domain.

To test this, the residual stress has been computed with local linear gyrokinetic calculations by imposing a finite constant tilting angle θ_0 to the mode structure. The result is presented in Fig. 5(a) as a function of the measured values of R/L_{ne} for the cases of TEM instabilities, where a negative tilting angle $\theta_0 = -0.3$ rad is applied to all of the cases. In qualitative agreement with the experimental observations, and with previous analytical derivations [25,29], it is found that the residual stress is large only in the presence of large values of R/L_{ne}. The Coriolis pinch term [30] is also plotted, and found to provide a small contribution for most of the database, due to the small Mach numbers. Finally, the total prediction for u' is computed, adding residual stress and pinch, by imposing $\Gamma_\phi = 0$ for intrinsic rotation conditions, and plotted also as a function of the measured u' in Fig. 5(b). A reasonable quantitative agreement with the observations is found, demonstrating that the main symmetry breaking mechanisms should produce values of θ_0 of the order of that applied in the simulations, and which do not vary much over the large parameter range covered by the present database. For the ITG cases, the value of θ_0 which provides a good match of the data for TEM yields too large negative values of u', and a better quantitative match is obtained instead with $\theta_0 \approx -0.15$ rad.

Analytical formulas [24] have been used and nonlinear simulations with the code GKW [26] of a subset of points have been performed to quantify the strength of the $E \times B$ shearing mechanism, assuming neoclassical poloidal rotation. It is found that it provides a significant contribution with respect to the measured values of u'. For the majority of cases, which have a negative shearing rate, this contribution is negative; that is, the residual stress is directed outward. Consistently with previous results [27], the nonlinear gyrokinetic simulations show that this contribution does not change sign when moving from TEM to ITG turbulence. Hence, this mechanism does not appear to be able to explain observations of positive values of u' in the presence of negative values of the shearing rate, which are found to be in the ITG instability domain, and cannot alone explain all of the observations. From linear global simulations [29], the profile shearing mechanism [27,29] predicts values of θ_0 which are in the same range as those required in GS2 to match the experimental values, and which change sign at the mode transition, predicting negative and positive values of u' in the TEM and ITG regimes, respectively. This mechanism could provide the required inward directed contribution to the residual stress in the ITG domain. Therefore, this analysis suggests that both $E \times B$ and profile shearing mechanisms should be at play, and can explain why in the database the reversal of u' from negative to positive is not observed exactly at the transition from TEM to ITG, but shifted to small positive values of ω_r, that is still close to the transition, but in the ITG domain. The location where the reversal of u' is observed with respect to the transition from TEM to ITG can provide an indirect indication of the relative strength of the two mechanisms. Finally, the quantitative agreement found in Fig. 5(b) suggests that at least the dominant part of these rather complex global effects can be appropriately encapsulated in theoretically founded parametrizations for the local descriptions required for core transport modelling.

In conclusion, the analysis of a large database of observations of intrinsic toroidal rotation, measured in different plasma conditions and confinement regimes in the AUG tokamak, indicates that countercurrent intrinsic toroidal rotation is produced in conditions where the logarithmic density gradients are sufficiently large and the turbulence regime is either in the TEM domain or close to the transition between ITG and TEM. The experimentally observed dependence is quantitatively reproduced by local linear gyrokinetic simulations, assuming a constant negative tilting angle over the database in the TEM domain. The analysis suggests that the dominant trend in the observations can be explained by the combination of residual stresses produced by $E \times B$ and profile shearing mechanisms. Detailed quantification of these mechanisms will require challenging nonlinear global simulations, which are left for future work. By the present results we propose a new framework within which previous and future experimental results obtained in other devices can be analyzed, in order to further validate, or invalidate, the characterization of the intrinsic toroidal rotation indicated by the present analysis.

The authors are grateful to Y. Camenen and A. G. Peeters for fruitful discussions.

[1] J. S. deGrassie *et al.*, Plasma Phys. Controlled Fusion **51**, 124047 (2009).
[2] A. G. Peeters *et al.*, Nucl. Fusion **51**, 094027 (2011).

[3] L.-G. Eriksson *et al.*, Plasma Phys. Controlled Fusion **39**, 27 (1997).
[4] J. E. Rice *et al.*, Nucl. Fusion **38**, 75 (1998).
[5] K. Itoh *et al.*, *Transport and Structural Formation in Plasmas* (Institute of Physics, London, 1999).
[6] A. Bortolon *et al.*, Phys. Rev. Lett. **97**, 235003 (2006).
[7] J. S. deGrassie *et al.*, Phys. Plasmas **14**, 056115 (2007).
[8] B. P. Duval *et al.*, Phys. Plasmas **15**, 056113 (2008).
[9] J. E. Rice *et al.*, Plasma Phys. Controlled Fusion **50**, 124042 (2008).
[10] J. E. Rice *et al.*, Nucl. Fusion **51**, 083005 (2011).
[11] R. M. McDermott *et al.*, Plasma Phys. Controlled Fusion **53** 124013 (2011).
[12] J. E. Rice *et al.*, Nucl. Fusion **47**, 1618 (2007).
[13] J. E. Rice *et al.*, Phys. Rev. Lett. **106**, 215001 (2011).
[14] J. S. deGrassie *et al.*, Nucl. Fusion **49**, 085020 (2009).
[15] C. Angioni *et al.*, Plasma Phys. Controlled Fusion **51**, 124017 (2009).
[16] W. Dorland *et al.*, Phys. Rev. Lett. **85**, 5579 (2000).
[17] C. Angioni *et al.*, Phys. Plasmas **12**, 040701 (2005).
[18] G. T. Hoang *et al.*, Phys. Rev. Lett. **93**, 135003 (2004).
[19] E. Fable *et al.*, Plasma Phys. Controlled Fusion **52**, 015007 (2010).
[20] C. Angioni *et al.*, Nucl. Fusion **51**, 023006 (2011).
[21] F. Romanelli *et al.*, Nucl. Fusion **26**, 1515 (1986).
[22] L. Lin *et al.*, Plasma Phys. Controlled Fusion **51**, 065006 (2009).
[23] R. R. Dominguez and G. M. Staebler, Phys. Fluids B **5**, 3876 (1993).
[24] O. D. Gurcan *et al.*, Phys. Plasmas **14**, 042306 (2007).
[25] P. H. Diamond *et al.*, Phys. Plasmas **15**, 012303 (2008).
[26] F. J. Casson *et al.*, Phys. Plasmas **16**, 092303 (2009).
[27] R. E. Waltz *et al.*, Phys. Plasmas **18**, 042504 (2011).
[28] O. D. Gurcan *et al.*, Phys. Plasmas **17**, 112309 (2010).
[29] Y. Camenen *et al.*, Nucl. Fusion **51**, 073039 (2011).
[30] A. G. Peeters, C. Angioni, and D. Strintzi, Phys. Rev. Lett. **98**, 265003 (2007).